USING THE METHOD OF FUNDAMENTAL SOLUTIONS IN CONJUNCTION WITH THE DEGENERATE KERNEL IN CYLINDRICAL ACOUSTIC PROBLEMS

I-Lin Chen

ABSTRACT

This paper proposes applications of the method of fundamental solutions (MFS) to exterior acoustic radiation and scattering problems. By using the two-point function of fundamental solutions, the coefficients of influence matrices are easily determined. It is found that this method also pordoces irregular frequencies as well as the boundary element method does. The position of the irregular frequency depends on the source point location. To avoid this numerical instability, the mixed-layer potential method is employed to deal with the problem. Based on the circulant properties and degenerate kernels, an analytical scheme in the discrete system of a cylinder is achieved to demonstrate the existence of irregular frequencies. Three numerical examples of uniform radiation, nonuniform radiation and scattering problems of a circular cylinder are examined and are compared with the results by using direct BEM.

Key Words: method of fundamental solutions, two-point function, irregular frequency, circulant, degenerate kernels.

I. INTRODUCTION

In numerical methods, mesh generation for complicated geometry is always time consuming in the stage of model creation for engineers dealing with engineering problems by employing the finite difference method (FDM), finite element method (FEM) or boundary element method (BEM).

Over the past decade, researchers have paid attention to the meshless method without employing the concept of elements. The initial idea of the meshless method dates back to the smooth particle hydrodynamics (SPH) method for modeling astrophysical phenomena (Gingold and Maraghan, 1977). Several meshless methods have also been reported in the literature, for example, the domain-based methods including the element-free Galerkin method (Belystcho *et al*., 1994), the reproducing kernel method (Liu *et al*., 1995), and boundary-based methods including the boundary node method (Mukherjee and Mukherjee, 1997), the meshless local Petrov-Galerkin approach (Atluri and Zhu, 1998), the local boundary integral equation method (Sladek *et al*., 2000), the RBF approach (Chen *et al*., 1998; Golberg *et al*., 2000; Zhang *et al*., 2000) and the method of fundamental solutions (MFS) (Kondapalli *et al*., 1992; Poullikkas *et al*., 2002). The MFS is a technique for the numerical solution of certain elliptic boundary value problems, and it may be viewed as an indirect boundary element method with a concentrated source instead of a distributed one (Chen *et al*., 2000). Like the boundary element method, it is applicable when a fundamental solution of the differential equation in question is known. The basic idea is to approximate the solution by forming a linear combination of fundamental solutions with sources located outside the problem domain. The coefficients of the linear combination are determined so that the approximate solution satisfies the problem boundary conditions. Poullikkas *et al*. (2002) employed MFS to solve three-dimensional electrostatics, and only a few sources were adopted. Cisilino and Sensale (2002) developed a simulated annealing algorithm for the Laplace equation, to decide the

I. L. Chen is with the Department of Naval Architecture, National Kaohsiung Marine University, Kaohsiung 811, Taiwan. (Tel: 886-7-3617141 ext. 3402; Fax: 886-7-3656481; Email: ilchen@mail.nkmu.edu.tw)

optimal position of source points by using the MFS. However, the drawback of the method is that it is complicated to compute and so the benefit of the MFS is lost. Ramachandran (2002) adopted the singular value decomposition (SVD) technique, by truncating the nearly zero singular value, to resolve the ill-posed problem in the MFS. Kondapalli *et al*. (1992) applied the MFS to acoustic scattering in fluids and solids. Further details are found in the review paper by Fairweather and Karageorghis (1998) on the MFS approach.

One of the problems frequently addressed in BEM is the problem of irregular (fictitious) frequencies for exterior acoustics. Kondapalli (1992) pointed out that the difficulty of fictitious frequencies appearing in the BEM is not present in the MFS. The reason is that a discrete set of source points does not define an internal surface uniquely, as quoted from Fairweather *et al*., 2003. In this paper, we will examine this point for the fictitious frequency phenomenon in the MFS.

The fictitious frequencies do not represent any kind of physical resonance but are due to the numerical method, which does not have a unique solution at some eigenfrequencies for corresponding interior problems (Dokumaci, 1990; Lee *et al*., 1996; Lee and Sclavounos, 1989; Malenica and Chen, 1998; Ohmatsu, 1983; Ursell, 1981). It was found that BEM results in fictitious eigenvalues, which are associated with the interior frequency of the Dirichlet problem. The general derivation has been provided by a continuous system (Chen, 1998), and a discrete system using a circulant (Kuo *et al*., 2000; Chen and Kuo, 2000). Following the retracted BEM formulation (Hwang and Chang, 1991), it was found that the position of the irregular frequency depends on the source location. Wilton *et al*., 1993, proved the equivalence between the superposition method and the layer potential method. Since the non-uniqueness problem exists in the layer potential method, fictitious frequencies also appear in the superposition method. In the numerical examples, they demonstrated the appearance of fictitious frequencies in three-dimensional cases in the superposition method. The MFS and the retracted BEM can be seen as similar indirect methods instead of the difference between a lump source and a distributed source.

The fictitious frequency in exterior acoustic problems is similar to the spurious eigenvalues which occur in the annular eigenproblem when the MFS is used. The positions of spurious eigenvalues for the annular problem depend on the location of the inner fictitious boundary when the sources are distributed (Chen *et al*., 2005). The spurious eigenvalues appearing in the single and double-layer MFS were found to be the interior eigenvalues corresponding to the Dirichlet and Neumann problems, respectively. A similar mechanism in exterior acoustics will be examined in this paper.

In order to obtain a unique solution that is known to exist analytically, several approaches for BEM that provide additional constraints to the original system of equations have been proposed. Burton and Miller (1971) proposed an integral equation that was valid for all wave numbers by forming a linear combination of the singular integral equation and its normal derivative. Numerical examples for nonuniform radiation problems using the dual BEM were provided and irregular frequencies were easily found (Chen *et al*., 2003). Although the fictitious frequencies can be predicted theoretically (Chen, 1998; Chen and Kuo, 2000), we may not find the positions of numerical instability from the real computations for some cases, and how to explain the reason for this is not trivial.

This paper will study the mechanism of fictitious-frequencies in exterior acoustics by using the MFS. An analytical study of the fictitious frequency in a discrete system for a circular cylinder is conducted by using the degenerate kernel and circulants. Three numerical examples of uniform radiation, nonuniform radiation and scattering problems of a circular cylinder are also examined and are compared with the analytical solution and the results from using the direct BEM.

II. THE MFS FORMULATION FOR HELMHOLTZ EQUATION

The boundary value problem to be solved can be stated as follows: The acoustic pressure $u(x)$ must satisfy the Helmholtz equation,

$$\nabla^2 u(x) + k^2 u(x) = 0,\ x \in D \tag{1}$$

where $k = \omega/c$ is the wave number and ω is the angular frequency and D is the domain of interest. By using the MFS, the acoustic field and flux can be described by linear combinations of fundamental solutions:

1. Single-Layer Potential Approach (*UL* Method)

$$u(x) = \sum_{j=1}^{2N} U(s_j, x)\Gamma(s_j) \tag{2}$$

$$t(x) = \sum_{j=1}^{2N} L(s_j, x)\Gamma(s_j) \tag{3}$$

2. Double-Layer Potential Approach (*TM* Method)

$$u(x) = \sum_{j=1}^{2N} T(s_j, x)\Omega(s_j) \tag{4}$$

$$t(x) = \sum_{j=1}^{2N} M(s_j, x)\Omega(s_j) \tag{5}$$

where x and s are the collocation and source points, respectively, as shown in Fig. 1, $L(s, x) \equiv \frac{\partial U(s, x)}{\partial n_x}$; $T(s, x) \equiv \frac{\partial U(s, x)}{\partial n_s}$; $M(s, x) \equiv \frac{\partial^2 U(s, x)}{\partial n_x \partial n_s}$; $t(\boldsymbol{x}) \equiv \frac{\partial u(s)}{\partial n_x}$, n is the normal vector; $\Gamma(s_j)$ and $\Omega(s_j)$ are the generalized unknowns for the densities of single and double-layer potential, respectively, at s_j; $2N$ is the number of collocation points; and $U(s, x)$ is the fundamental solution, which satisfies

$$\nabla^2 U(s, x) + k^2 U(s, x) = 2\pi\delta(s - x) \tag{6}$$

in which δ is the Dirac delta function. The four kernels are,

$$U(s, x) = \frac{-i\pi}{2} H_0^{(1)}(kr) \tag{7}$$

$$T(s, x) = \frac{\partial U(s, x)}{\partial n_s} = \frac{i\pi k}{2} \frac{H_1^{(1)}(kr) y_i n_i}{r} \tag{8}$$

$$L(s, x) = \frac{\partial U(s, x)}{\partial n_x} = \frac{-i\pi k}{2} \frac{H_1^{(1)}(kr) y_j \overline{n}_j}{r} \tag{9}$$

$$M(s, x) = \frac{\partial^2 U(s, x)}{\partial n_s \partial n_x}$$

$$= \frac{-i\pi k}{2} \frac{-kH_2^{(1)}(kr) y_i y_j n_i \overline{n}_j}{r^2} + \frac{H_1^{(1)}(kr) n_i \overline{n}_i}{r}) \tag{10}$$

where $r \equiv |s - x|$ is the distance between the source and collocation points; $\overline{n}_i$ is the ith component of the outnormal vector at x; n_i is the ith component of the outnormal vector at s; $H_n^{(1)}$ denotes the first kind of the nth order Hankel functions; and $y_i \equiv s_i - x_i$, $i = 1, 2$, are the differences of the ith components of s and x.

We consider an infinite circular cylinder with the Dirichlet boundary condition

$$u(x) = \overline{u},\ x \in B \tag{11}$$

where B is the boundary.

By matching the boundary conditions for x on the $2N$ boundary points into Eqs. (2) and (3) we have

$$\{\overline{u}\} = [\boldsymbol{U}]\{\boldsymbol{\Gamma}\} \tag{12}$$

$$\{t\} = [\boldsymbol{L}]\{\boldsymbol{\Gamma}\} \tag{13}$$

where $\{\Gamma\}$ is the vectors of undetermined coefficients. If k is not the fictitious frequency, Eq. (12) can be rearranged to

$$\{\Gamma\} = \{\boldsymbol{U}\}^{-1}\{\overline{\boldsymbol{u}}\} \tag{14}$$

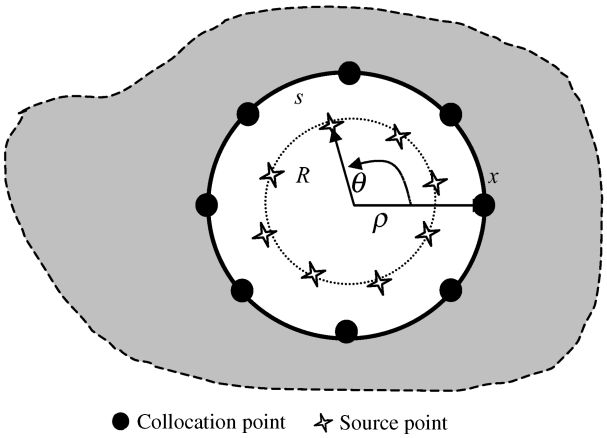

Fig. 1 The located position of source and collocation point and definitions of ρ, θ, R and r

We obtain the unknown boundary density $\{t\}$ as follows:

$$\{t\} = [\boldsymbol{L}][\boldsymbol{U}]^{-1}\{\overline{\boldsymbol{u}}\} = [\boldsymbol{SD}]\{\overline{\boldsymbol{u}}\} \tag{15}$$

where $[SD] = [\boldsymbol{L}][\boldsymbol{U}]^{-1}$ denotes the matrix by using the Single-layer potential approach for the Dirichlet problem. By substituting Eq. (14) into Eq.(2), we obtain the field pressure

$$u(x) = \langle w(x) \rangle [\boldsymbol{U}]^{-1}\{\overline{\boldsymbol{u}}\} \tag{16}$$

where $\langle w \rangle$ is the influence row vector of the field point obtained by using the $U(s, x)$ kernel.

Now, we consider another case with the Neumann boundary conditions

$$t(x) = \overline{t},\ x \in B \tag{17}$$

By matching the boundary conditions for x on the $2N$ boundary points into Eq. (3), we have

$$\{\overline{t}\} = [\boldsymbol{L}]\{\boldsymbol{\Gamma}\} \tag{18}$$

and Eq. (18) can be rearranged to

$$\{\Gamma\} = [\boldsymbol{L}]^{-1}\{\overline{\boldsymbol{t}}\}. \tag{19}$$

We obtain the unknown boundary density $\{u\}$ as follows:

$$\{u\} = [\boldsymbol{U}][\boldsymbol{L}]^{-1}\{\overline{\boldsymbol{t}}\} = [\boldsymbol{SN}]\{\overline{\boldsymbol{t}}\} \tag{20}$$

where $[SN] = [\boldsymbol{U}][\boldsymbol{L}]^{-1}$ denotes the matrix by using the Single-layer potential approach for the Neumann problem. By substituting Eq. (19) into Eq. (2), we obtain the field pressure for the Neumann boundary condition

$$u(x) = \langle w(x) \rangle [\boldsymbol{L}]^{-1}\{\overline{\boldsymbol{t}}\} \tag{21}$$

Similarly, by matching the boundary conditions for x on the $2N$ boundary points into Eq. (4), we have

$$\{\bar{u}\} = [\boldsymbol{T}]\{\boldsymbol{\Omega}\} \tag{22}$$

where $\{\Omega\}$ represents the vectors of undetermined coefficients. Eq. (22) can be rearranged to

$$\{\boldsymbol{\Omega}\} = [\boldsymbol{T}]^{-1}\{\bar{\boldsymbol{u}}\} \tag{23}$$

We can obtain the unknown boundary density $\{t\}$ as follows:

$$\{t\} = [\boldsymbol{M}][\boldsymbol{T}]^{-1}\{\bar{\boldsymbol{u}}\} = [\boldsymbol{DD}]\{\bar{\boldsymbol{u}}\} \tag{24}$$

where $[\boldsymbol{DD}] = [\boldsymbol{M}][\boldsymbol{T}]^{-1}$ denotes the matrix, by using the Double-layer potential approach for the Dirichlet problem. By substituting Eq. (23) into Eq.(4), we obtain the field pressure

$$u(x) = <\upsilon(x)> [\boldsymbol{T}]^{-1}\{\bar{\boldsymbol{u}}\}, \tag{25}$$

where $<\upsilon>$ is the influence row vector of the field point obtained by using the $T(s, x)$ kernel. Similarly, considering the Neumann boundary condition, $t(x) = \bar{t}$, we have

$$\{\bar{\boldsymbol{t}}\} = [\boldsymbol{M}]\{\boldsymbol{\Omega}\} \tag{26}$$

Eq. (26) can be rearranged to

$$\{\boldsymbol{\Omega}\} = [\boldsymbol{M}]^{-1}\{\bar{\boldsymbol{t}}\} \tag{27}$$

We can obtain the unknown boundary density $\{u\}$ as follows:

$$\{u\} = [\boldsymbol{T}][\boldsymbol{M}]^{-1}\{\bar{\boldsymbol{t}}\} = [\boldsymbol{DN}]\{\bar{\boldsymbol{t}}\} \tag{28}$$

where $[DN] = [\boldsymbol{T}][\boldsymbol{M}]^{-1}$ denotes the matrix by using the Double-layer potential approach for the Neumann problem. By substituting Eq. (27) into Eq.(4), we obtain the field pressure for the Neumann boundary condition

$$u(x) = <\upsilon(x)> [\boldsymbol{M}]^{-1}\{\bar{\boldsymbol{u}}\} \tag{29}$$

III. ANALYTICAL STUDY OF THE IRREGULAR FREQUENCY FOR THE CIRCULAR RADIATOR USING CIRCULANTS IN THE DISCRETE SYSTEM

For the circular case, we can express $x = (\rho, \phi)$ and $s = (R, \theta)$ in terms of polar coordinates. The four kernels can be expressed in terms of degenerate kernels as shown below:

$$U(s, x) = \begin{cases} U^i(R, \theta; \rho, \phi) = \sum_{n=-\infty}^{n=\infty} \frac{\pi}{2}[-iJ_n(kR) + Y_n(kR)]J_n(k\rho)\cos(n(\theta-\phi)), & R > \rho \\ U^e(R, \theta; \rho, \phi) = \sum_{n=-\infty}^{n=\infty} \frac{\pi}{2}[-iJ_n(k\rho) + Y_n(k\rho)]J_n(kR)\cos(n(\theta-\phi)), & R < \rho \end{cases} \tag{30}$$

$$T(s, x) = \begin{cases} T^i(R, \theta; \rho, \phi) = \sum_{n=-\infty}^{n=\infty} \frac{k\pi}{2}[-iJ'_n(kR) + Y'_n(kR)]J_n(k\rho)\cos(n(\theta-\phi)), & R > \rho \\ T^e(R, \theta; \rho, \phi) = \sum_{n=-\infty}^{n=\infty} \frac{k\pi}{2}[-iJ_n(k\rho) + Y_n(k\rho)]J'_n(kR)\cos(n(\theta-\phi)), & R < \rho \end{cases} \tag{31}$$

$$L(s, x) = \begin{cases} L^i(R, \theta; \rho, \phi) = \sum_{n=-\infty}^{n=\infty} \frac{k\pi}{2}[-iJ_n(kR) + Y_n(kR)]J'_n(k\rho)\cos(n(\theta-\phi)), & R > \rho \\ L^e(R, \theta; \rho, \phi) = \sum_{n=-\infty}^{n=\infty} \frac{k\pi}{2}[-iJ'_n(k\rho) + Y'_n(k\rho)]J_n(kR)\cos(n(\theta-\phi)), & R < \rho \end{cases} \tag{32}$$

$$M(s, x) = \begin{cases} M^i(R, \theta; \rho, \phi) = \sum_{n=-\infty}^{n=\infty} \frac{k^2\pi}{2}[-iJ'_n(kR) + Y'_n(kR)]J'_n(k\rho)\cos(n(\theta-\phi)), & R > \rho \\ M^e(R, \theta; \rho, \phi) = \sum_{n=-\infty}^{n=\infty} \frac{k^2\pi}{2}[-iJ'_n(k\rho) + Y'_n(k\rho)]J'_n(kR)\cos(n(\theta-\phi)), & R < \rho \end{cases} \tag{33}$$

where J_n and Y_n are the first and second Bessel functions with order n, and the superscripts "i" and "e" denote the interior ($R > \rho$) and exterior domains ($R < \rho$), respectively.

Since the rotation symmetry is preserved for a circular boundary, the four influence matrices in Eqs. (2)-(5) are denoted by $[\boldsymbol{U}]$, $[\boldsymbol{L}]$, $[\boldsymbol{T}]$ and $[\boldsymbol{M}]$ of the circulants with the elements

$$K_{ij} = K(R,\ \theta_j;\ \rho,\ \phi_i) \tag{34}$$

where the kernel K can be U, T, L or M, ϕ_i and θ_j are the angles of observation and source points, respectively. By superimposing $2N$ lumped strength along the boundary, we have the influence matrices,

$$[\boldsymbol{K}] = \begin{bmatrix} a_0 & a_1 & a_2 & \cdots & a_{2N-2} & a_{2N-1} \\ a_{2N-1} & a_0 & a_1 & \cdots & a_{2N-3} & a_{2N-2} \\ a_{2N-2} & a_{2N-1} & a_0 & \cdots & a_{2N-4} & a_{2N-3} \\ \vdots & \vdots & \vdots & \ddots & \vdots & \vdots \\ a_1 & a_2 & a_3 & \cdots & a_{2N-1} & a_0 \end{bmatrix} \tag{35}$$

where the elements of the first row can be obtained by

$$a_{j-i} = K(s_j,\ x_i) \tag{36}$$

The matrix $[\boldsymbol{K}]$ in Eq. (35) is found to be a circulant since the rotational symmetry for the influence coefficients is considered. By introducing the following bases for the circulants, I, $(C_{2N})^1$, $(C_{2N})^2$, $\cdots$, and $(C_{2N})^{2N-1}$, we can expand $[\boldsymbol{K}]$ into

$$[K] = a_0 I + a_1 (C_{2N})^1 + a_2 (C_{2N})^2 + \ldots + a_{2N-1} (C_{2N})^{2N-1} \tag{37}$$

where I is a unit matrix and

$$C_{2N} = \begin{bmatrix} 0 & 1 & 0 & \cdots & 0 & 0 \\ 0 & 0 & 1 & \cdots & 0 & 0 \\ \vdots & \vdots & \vdots & \ddots & \vdots & \vdots \\ 0 & 0 & 0 & \cdots & 0 & 1 \\ 1 & 0 & 0 & \cdots & 0 & 0 \end{bmatrix}_{2N \times 2N} \tag{38}$$

Based on the circulant theory, the eigenvalues for the influence matrix, $[\boldsymbol{K}]$, are found as follows:

$$\lambda_\ell = a_0 + a_1 \alpha_\ell + a_2 \alpha_\ell^2 + \cdots + a_{2N-1} \alpha_\ell^{2N-1},$$
$$\ell = 0,\ \pm 1,\ \pm 2,\ \ldots,\ \pm (N-1),\ N \tag{39}$$

where λ_ℓ and α_ℓ are the eigenvalues for $[\boldsymbol{K}]$ and $[C_{2N}]$, respectively. It is easily found that the eigenvalues for the circulant $[C_{2N}]$ are the roots for $\alpha^{2N} = 1$ as shown below:

$$\alpha_\ell = e^{i\frac{2\pi\ell}{2N}},\ \ell = 0, \pm 1, \pm 2, \cdots, \pm (N-1), N \text{ or}$$
$$\ell = 0,\ 1,\ 2,\ \cdots,\ 2N-1 \tag{40}$$

Substituting Eq. (40) into Eq. (39), we have

$$\lambda_\ell = \sum_{m=0}^{2N-1} a_m \alpha_\ell^m = \sum_{m=0}^{2N-1} a_m e^{i\frac{2\pi}{2N} m\ell},$$
$$\ell = 0, \pm 1, \pm 2, \cdots, \pm (N-1), N \tag{41}$$

According to the definition for a_m in Eq. (36), we have

$$a_m = a_{2N-m},\ \ m = 0,\ 1,\ 2,\ \cdots,\ 2N-1 \tag{42}$$

Substituting Eq. (42) into Eq. (41) yields

$$\lambda_\ell = a_0 + (-1)^\ell a_N + \sum_{m=1}^{N-1} (\alpha_\ell^m + \alpha_\ell^{2N-m}) a_m = \sum_{m=0}^{2N-1} \cos(m\ell\Delta\theta) a_m \tag{43}$$

Putting Eq. (36) into Eq. (43) for the case U of K for $\phi = 0$ without loss of generality, the Reimann sum of infinite terms reduces to the following integral

$$\lambda_\ell = \lim_{N\to\infty} \sum_{m=0}^{2N-1} \cos(m\ell\Delta\theta) U(m\Delta\theta, 0) \approx \frac{1}{\rho\Delta\theta} \int_0^{2\pi} \cos(\ell\theta) U(\theta, 0) \rho d\theta \tag{44}$$

where $\Delta\theta = \frac{2\pi}{2N}$. By using the degenerate kernel for $U(s, x)$ in Eq. (30) and the orthogonal conditions, Eq. (40) reduces to

$$\lambda_\ell = -i\pi^2 \rho H_\ell^{(1)}(k\rho) J_\ell(kR),$$
$$\ell = 0, \pm 1, \pm 2, \cdots, \pm (N-1), N \tag{45}$$

Similarly, we have

$$\mu_\ell = -ik\pi^2 \rho H_\ell'^{(1)}(k\rho) J_\ell(kR)$$
$$\ell = 0, \pm 1, \pm 2, \cdots, \pm (N-1), N \tag{46}$$

$$\nu_\ell = -ik\pi^2 \rho H_\ell^{(1)}(k\rho) J_\ell'(kR)$$
$$\ell = 0, \pm 1, \pm 2, \cdots, \pm (N-1), N \tag{47}$$

$$\kappa_\ell = -ik^2\pi^2 \rho H_\ell'^{(1)}(k\rho) J_\ell'(kR)$$
$$\ell = 0, \pm 1, \pm 2, \cdots, \pm (N-1), N \tag{48}$$

where μ, ν and κ are the eigenvalues of $[\boldsymbol{L}]$, $[\boldsymbol{T}]$ and $[\boldsymbol{M}]$ matrices, respectively. The determinants for the four matrices are obtained by multiplying all the eigenvalues as shown below:

$$\det[U] = \lambda_0 (\lambda_1 \lambda_2 \cdots \lambda_{N-1})^2 \lambda_N \tag{49}$$

$$\det[L] = \mu_0 (\mu_1 \mu_2 \cdots \mu_{N-1})^2 \mu_N \tag{50}$$

$$\det[T] = \nu_0 (\nu_1 \nu_2 \cdots \nu_{N-1})^2 \nu_N \tag{51}$$

$$\det[M] = \kappa_0(\kappa_1\kappa_2 \cdots \kappa_{N-1})^2\kappa_N \tag{52}$$

Since the four matrices [$\boldsymbol{U}$], [$\boldsymbol{L}$], [$\boldsymbol{T}$] and [$\boldsymbol{M}$] are all symmetric circulants, they can be expressed by

[$\boldsymbol{U}$]

$$= \boldsymbol{\Phi}\begin{bmatrix} \lambda_0 & 0 & 0 & \cdots & 0 & 0 & 0 \\ 0 & \lambda_1 & 0 & \cdots & 0 & 0 & 0 \\ 0 & 0 & \lambda_{-1} & \cdots & 0 & 0 & 0 \\ \vdots & \vdots & \vdots & \ddots & \vdots & \vdots & \vdots \\ 0 & 0 & 0 & \cdots & \lambda_{(N-1)} & 0 & 0 \\ 0 & 0 & 0 & \cdots & 0 & \lambda_{-(N-1)} & 0 \\ 0 & 0 & 0 & \cdots & 0 & 0 & \lambda_N \end{bmatrix}_{2N\times 2N} \boldsymbol{\Phi}^{-1} \tag{53}$$

[$\boldsymbol{L}$]

$$= \boldsymbol{\Phi}\begin{bmatrix} \mu_0 & 0 & 0 & \cdots & 0 & 0 & 0 \\ 0 & \mu_1 & 0 & \cdots & 0 & 0 & 0 \\ 0 & 0 & \mu_{-1} & \cdots & 0 & 0 & 0 \\ \vdots & \vdots & \vdots & \ddots & \vdots & \vdots & \vdots \\ 0 & 0 & 0 & \cdots & \mu_{(N-1)} & 0 & 0 \\ 0 & 0 & 0 & \cdots & 0 & \mu_{-(N-1)} & 0 \\ 0 & 0 & 0 & \cdots & 0 & 0 & \mu_N \end{bmatrix}_{2N\times 2N} \boldsymbol{\Phi}^{-1} \tag{54}$$

[$\boldsymbol{T}$]

$$= \boldsymbol{\Phi}\begin{bmatrix} \mu_0 & 0 & 0 & \cdots & 0 & 0 & 0 \\ 0 & \nu_1 & 0 & \cdots & 0 & 0 & 0 \\ 0 & 0 & \nu_{-1} & \cdots & 0 & 0 & 0 \\ \vdots & \vdots & \vdots & \ddots & \vdots & \vdots & \vdots \\ 0 & 0 & 0 & \cdots & \nu_{(N-1)} & 0 & 0 \\ 0 & 0 & 0 & \cdots & 0 & \nu_{-(N-1)} & 0 \\ 0 & 0 & 0 & \cdots & 0 & 0 & \nu_N \end{bmatrix}_{2N\times 2N} \boldsymbol{\Phi}^{-1} \tag{55}$$

[$\boldsymbol{M}$]

$$= \boldsymbol{\Phi}\begin{bmatrix} \kappa_0 & 0 & 0 & \cdots & 0 & 0 & 0 \\ 0 & \kappa_1 & 0 & \cdots & 0 & 0 & 0 \\ 0 & 0 & \kappa_{-1} & \cdots & 0 & 0 & 0 \\ \vdots & \vdots & \vdots & \ddots & \vdots & \vdots & \vdots \\ 0 & 0 & 0 & \cdots & \kappa_{(N-1)} & 0 & 0 \\ 0 & 0 & 0 & \cdots & 0 & \kappa_{-(N-1)} & 0 \\ 0 & 0 & 0 & \cdots & 0 & 0 & \kappa_N \end{bmatrix}_{2N\times 2N} \boldsymbol{\Phi}^{-1} \tag{56}$$

where $\boldsymbol{\Phi}$ is the unitary matrix.

1. Derivation of Fictitious Frequency by Using the Single-Layer Potential Approach

For the Dirichlet problem, by employing Eqs. (53) and (54) for Eq.(15), we have

[$\boldsymbol{SD}$]

$$= \boldsymbol{\Phi}\begin{bmatrix} \sigma_0^{(SD)} & 0 & 0 & \cdots & 0 & 0 & 0 \\ 0 & \sigma_1^{(SD)} & 0 & \cdots & 0 & 0 & 0 \\ 0 & 0 & \sigma_{-1}^{(SD)} & \cdots & 0 & 0 & 0 \\ \vdots & \vdots & \vdots & \ddots & \vdots & \vdots & \vdots \\ 0 & 0 & 0 & \cdots & \sigma_{(N-1)}^{(SD)} & 0 & 0 \\ 0 & 0 & 0 & \cdots & 0 & \sigma_{-(N-1)}^{(SD)} & 0 \\ 0 & 0 & 0 & \cdots & 0 & 0 & \sigma_N^{(SD)} \end{bmatrix} \boldsymbol{\Phi}^{-1} \tag{57}$$

where the superscript "SD" denotes using the single-layer potential approach for the Dirichlet problem and

$$\sigma_\ell^{(SD)} = \frac{H_\ell'^{(1)}(ka)J_\ell(kR)}{H_\ell^{(1)}(ka)J_\ell(kR)},$$

$$\ell = 0, \pm1, \pm2, \cdots, \pm(N-1), N \tag{58}$$

where a is the radius of the circular cylinder. According to Eqs. (57) and (58), we have

$$\det[SD]$$

$$= \det[\boldsymbol{\Phi}]\sigma_0^{(SD)}(\sigma_1^{(SD)}\sigma_2^{(SD)}\cdots\sigma_{N-1}^{(SD)})^2\sigma_N^{(SD)}\det\left|\boldsymbol{\Phi}^{-1}\right|$$

$$= \sigma_0^{(SD)}(\sigma_1^{(SD)}\sigma_2^{(SD)}\cdots\sigma_{N-1}^{(SD)})^2\sigma_N^{(SD)} \tag{59}$$

since $\det|\boldsymbol{\Phi}| = \det|\boldsymbol{\Phi}^{-1}| = 1$. Based on Eq. (58), the numerical instability of zero divided by zero occurs at the denominator where k satisfies

$$H_\ell^{(1)}(ka)J_\ell(kR) = 0,\ \ell = 0, \pm1, \pm2, \cdots, \pm(N-1), N \tag{60}$$

Since the term of $H_\ell^{(1)}(ka)$ is never zero for any value of k, the k value satisfying Eq. (60), implies

$$J_\ell(kR) = 0 \tag{61}$$

For the Neumann problem, by employing Eqs. (53) and (54) for Eq. (20), we have

$$[SN] = \boldsymbol{\Phi} \begin{bmatrix} \sigma_0^{(SN)} & 0 & 0 & \cdots & 0 & 0 & 0 \\ 0 & \sigma_1^{(SN)} & 0 & \cdots & 0 & 0 & 0 \\ 0 & 0 & \sigma_{-1}^{(SN)} & \cdots & 0 & 0 & 0 \\ \vdots & \vdots & \vdots & \ddots & \vdots & \vdots & \vdots \\ 0 & 0 & 0 & \cdots & \sigma_{(N-1)}^{(SN)} & 0 & 0 \\ 0 & 0 & 0 & \cdots & 0 & \sigma_{-(N-1)}^{(SN)} & 0 \\ 0 & 0 & 0 & \cdots & 0 & 0 & \sigma_N^{(SN)} \end{bmatrix} \boldsymbol{\Phi}^{-1} \tag{62}$$

where the superscript "SN" denotes the Neumann problem using the single-layer potential approach and

$$\sigma_\ell^{(SN)} = \frac{H_\ell^{(1)}(ka) J_\ell(kR)}{H_\ell'^{(1)}(ka) J_\ell(kR)}, \quad \ell = 0, \pm 1, \pm 2, \cdots, \pm (N-1), N \tag{63}$$

According to Eqs. (62) and (63), we have

$$\begin{aligned} &\det[SN] \\ &= \det[\boldsymbol{\Phi}] \sigma_0^{(SN)} (\sigma_1^{(SN)} \sigma_2^{(SN)} \cdots \sigma_{N-1}^{(SN)})^2 \sigma_N^{(SN)} \det \left| \boldsymbol{\Phi}^{-1} \right| \\ &= \sigma_0^{(SN)} (\sigma_1^{(SN)} \sigma_2^{(SN)} \cdots \sigma_{N-1}^{(SN)})^2 \sigma_N^{(SN)} \end{aligned} \tag{64}$$

Based on Eq. (63), the numerical instability of zero divided by zero occurs at the denominator where k satisfies

$$H_\ell'^{(1)}(ka) J_\ell(kR) = 0, \ \ell = 0, \pm 1, \pm 2, \cdots, \pm (N-1), N \tag{65}$$

Since the term $H_\ell'^{(1)}(ka)$ is never zero for any value of k, the k value satisfying Eq. (65), implies

$$J_\ell(kR) = 0 \tag{66}$$

2. Derivation of Fictitious Frequency by Using the Double-Layer Potential Approach

Similarly, for the Dirichlet problem, by employing Eqs. (55) and (56) for Eq. (24), we have

$$\sigma_\ell^{(DD)} = \frac{H_\ell'^{(1)}(ka) J_\ell'(kR)}{H_\ell^{(1)}(ka) J_\ell'(kR)}, \quad \ell = 0, \pm 1, \pm 2, \cdots, \pm (N-1), N \tag{67}$$

where the superscript "DD" denotes the Dirichlet problem using the double-layer potential approach. Based on Eq. (67), the numerical instability of zero divided by zero occurs at the denominator where k satisfies

$$H_\ell^{(1)}(ka) J_\ell'(kR) = 0, \ \ell = 0, \pm 1, \pm 2, \cdots, \pm (N-1), N \tag{68}$$

For any value of k, the k value satisfying Eq. (68), implies

$$J_\ell'(kR) = 0 \tag{69}$$

For the Neumann problem, by employing Eqs. (55) and (56) for Eq. (28), we have

$$\sigma_\ell^{(DN)} = \frac{H_\ell^{(1)}(ka) J_\ell'(kR)}{H_\ell'^{(1)}(ka) J_\ell'(kR)}, \quad \ell = 0, \pm 1, \pm 2, \cdots, \pm (N-1), N \tag{70}$$

where the superscript "DN" denotes the Neumann problem using the double-layer potential approach. Based on Eq. (70), the numerical instability of zero divided by zero occurs at the denominator where k satisfies

$$H_\ell'^{(1)}(ka) J_\ell'(kR) = 0, \ \ell = 0, \pm 1, \pm 2, \cdots, \pm (N-1), N \tag{71}$$

For any value of k, the k value satisfying Eq. (71), implies

$$J_\ell'(kR) = 0 \tag{72}$$

After obtaining all the fictitious values which occur in each method, it is found that once the method of integral formulation (either, *UL* or *TM* method) is adopted, the positions of fictitious values are independent of the types of boundary condition.

The irregular frequency appears at the eigenvalue of the interior problem with the fictitious boundary of radius,"R", instead of the real boundary "a" in the direct BEM. The fictitious frequency "k_f^M" in the MFS can be obtained analytically for an infinite cylinder as follows

$$k_f^M = \frac{k_f a}{R} \tag{73}$$

where $k_f a = k_0$, k_0 is the root of the $J_\ell(k_0) = 0$ for the single-layer potential approach, or the root of the $J_\ell'(k_0) = 0$ for the double-layer potential approach. The occurring mechanism of the fictitious frequency can extend to the three-dimensional case easily.

The fictitious frequency was not found in

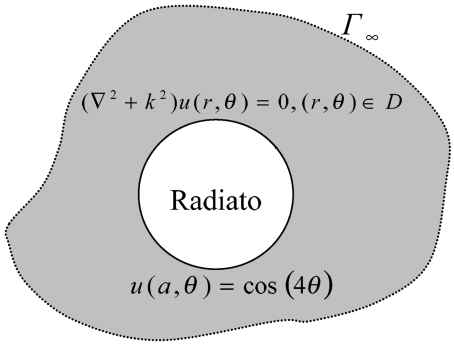

Fig. 2 The radiation problem (Dirichlet type) for a cylinder

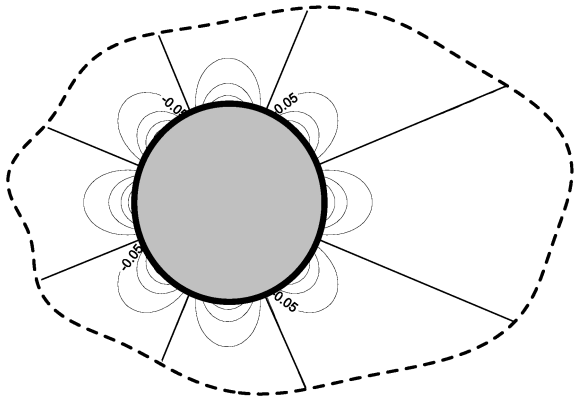

Fig. 3 The contour plot for the real-part solutions

Kondapalli *et al.*, 1992. The reason cited was that the fictitious frequencies in the MFS are different from those of derived BEM by a ratio of 2, since the radius of the sphere connected by the source points is half of the real boundary. The first fictitious frequency for the three-dimensional case occurs at the position of $k = 2\pi$, instead of $k = \pi$ in the BEM. That is the reason why they could not find the fictitious frequencies in the range of $0 < k < 5$.

IV. MIXED-LAYER POTENTIAL METHOD

In the exterior acoustics of the Helmholtz equation using dual BEM, the mixed-layer potential method (Hwang and Chang, 1991) utilized the product of double-layer equations with an imaginary constant to the single-layer equation to deal with the fictitious frequency which is the non-unique solution problem. We will extend this concept to MFS.

$$u(x_i) = \sum_j (U(s_j, x_i) + \frac{i}{k} T(s_j, x_i))\varphi(s_j) \tag{74}$$

$$t(x_i) = \sum_j (L(s_j, x_i) + \frac{i}{k} M(s_j, x_i))\varphi(s_j) \tag{75}$$

where φ is the mixed potential.

V. NUMERICAL EXAMPLES

Case 1: Uniform radiation from an infinite circular cylinder (Dirichlet boundary condition)

For the first example, a radiation problem is considered. The boundary condition is shown in Fig. 2. The normalized analytical solution to this cylinder problem with a radius $a = 1.0$ m is

$$u(\rho, \phi) = \frac{H_4^{(1)}(k\rho)}{H_4^{(1)}(ka)} \cos(4\phi)\ ,\ \rho \geq a,\ 0 \leq \varphi < 2\pi \tag{76}$$

subjected to boundary condition $u(a, \phi) = \cos(4\phi)$,

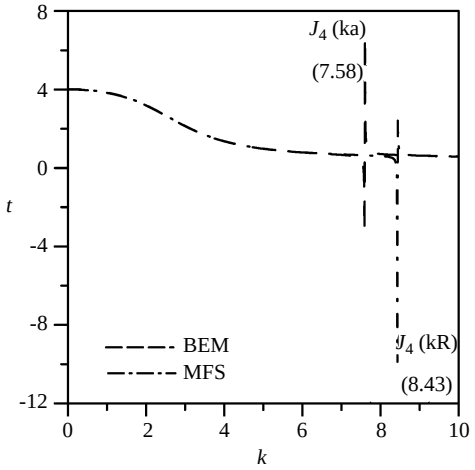

Fig. 4 The $t(a, 0)$ versus k for by using the MFS and BEM

where $H_4^{(1)}(k\rho)$ denotes the first-kind Hankel function of the fourth order. Sixty source points and sixty collocation points are adopted. The source points are located at $R = 0.9$ *m*. Fig. 3 shows the contour plot for the real-part solutions with $ka = 1.0$. The positions where the irregular values occur can be found, are showing in Fig. 4 for the solution t versus k at the position $a = 1$, $\phi = 0$ by using the MFS method and direct BEM. It is found that no irregular values can be found between zero and eight. At the position of $k \approx 8.43$, the numerical instability appears, since the value is the first zero of $J_4(kR)$ for the MFS method. The irregular value occurs at $k \approx 7.58$ when using the direct BEM. The fictitous frequency of the MFS differs from the value of direct BEM by a ratio of $\frac{7.58}{8.43} \approx 0.9$, as predicted analytically. The performance of the MFS in comparison with the analytical solution, and the mixed-layer potential approach is quite good, as shown in Fig. 5.

Case 2: Nonuniform radiation from an infinite circular cylinder (Neumann boundary condition)

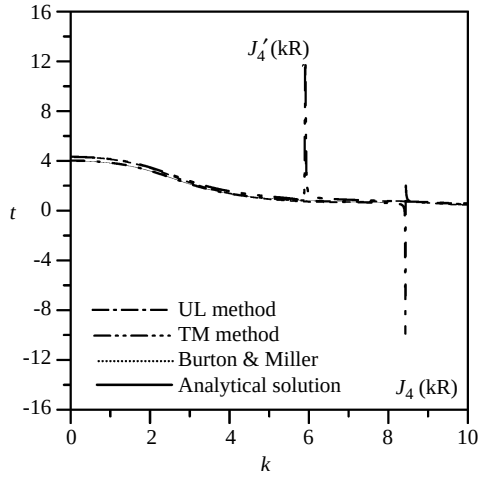

Fig. 5 The $t(a, 0)$ versus k for the uniform radiation problem

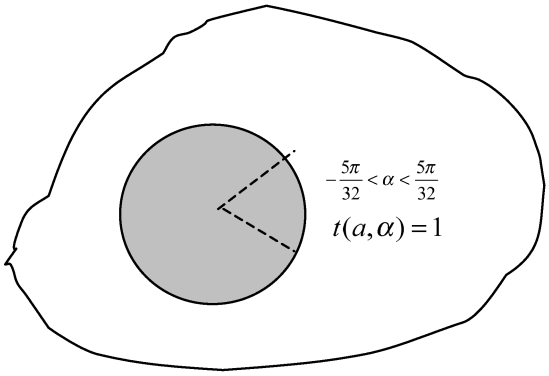

Fig. 6 The nonuniform radiation problem (Neumann type) for a cylinder

This problem was chosen because the exact solution is known (Harari *et al.*, 1998). The boundary condition is shown in Fig. 6. In this example we computed the nonuniform radiation from an infinite circular cylinder, and the Neumann boundary condition is applied to the cylinder surface. The portion ($-\alpha < \theta < \alpha$) is assigned a unit value, while the remaining portion is assigned a homogeneous value. The analytical solution to this cylinder problem with a radius a = 1.0 m is given by

$$u(\rho, \phi) = \frac{2}{\pi} \sum_{n=0}^{\infty}{}' \frac{-1}{k} \frac{\sin(n\alpha)}{n} \frac{H_n^{(1)}(k\rho)}{H_n^{(1)\prime}(ka)} \cos(n\phi) ,$$

$$\rho > a,\ 0 < \phi < 2\pi \qquad (77)$$

where the symbol ‘denotes that the first term (n = 0) is halved. We select $\alpha = \frac{5\pi}{16}$, and ka = 1. Fig. 7 shows the contour plots for the real part of the numerical solutions. Sixty-four nodes are adoped in the MFS and $\alpha = \frac{5\pi}{16}$ for this case. The source points are located at R = 0.9 m. The positions where the irregular

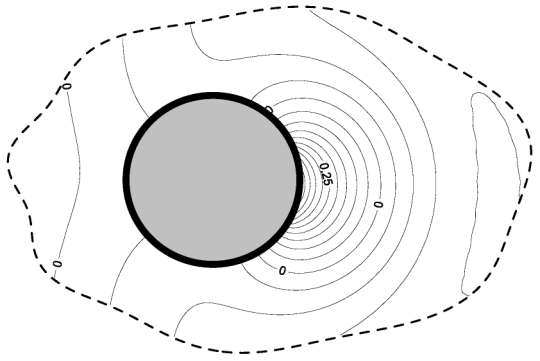

Fig. 7 The numerical solution for the nonuniform radiation problem (ka = 1, $\alpha = \frac{\pi}{9}$)

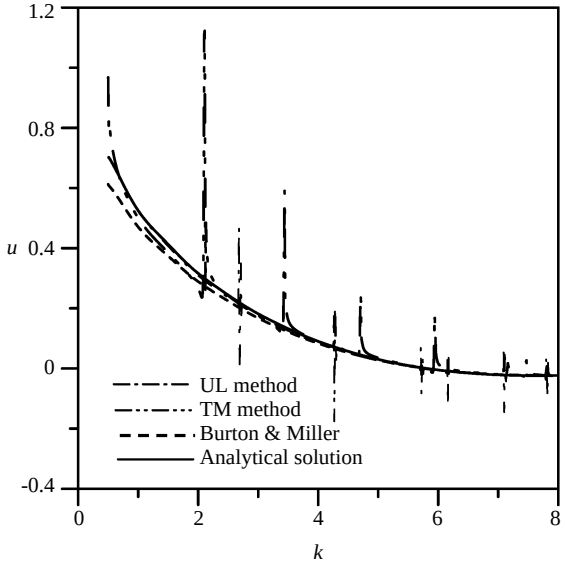

Fig. 8 The $u(a, 0; k)$ versus k using the MFS for the nonuniform radiation by a circular cylinder

values occur can be found in Fig. 8 for the solution u (a, 0; k) versus k. It is found that by using the *UL* formulation the irregular values occur at the positions of $J_{n,m}$, which is the mth zero of $J_n(kR)$. The fictitious frequencies which occurred at the position are described in Eq. (61). By using the *TM* formulation the irregular values occur at the positions of $J'_{n,m}$, which is the mth zero of $J'_n(kR)$. The results of the MFS, the mixed-layer potential approach and analytical solution are shown in Fig. 8. Figs. 9(a)-(c) show the surface potential for k = 1.0 by using the *UL*, *TM* and mixed-layer potential, respectively. The results of Fig. 9c, are worse than those of Figs. 9a and 9b. Although the three results are different, they all can be acceptable from a numerical viewpoint. Figs. 10(a)-(c) show the surface potential for k = 2.67 by using the *UL*, *TM* and mixed-layer potential, respectively, which corresponds to the first interior Dirichlet eigenproblem. In Fig. 10 (a) the result using the *UL* formulation shows some

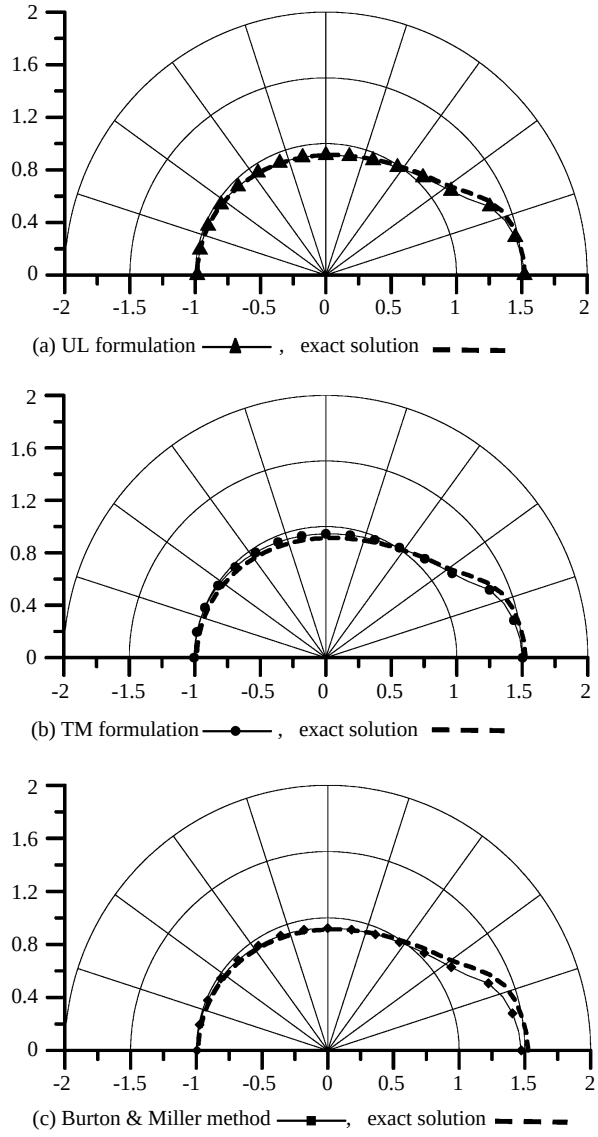

Fig. 9 Surface potential produced by the finite cylinder at ka = 1.0, (a) UL formulation, (b) TM formulation, (c) Burton & Miller method

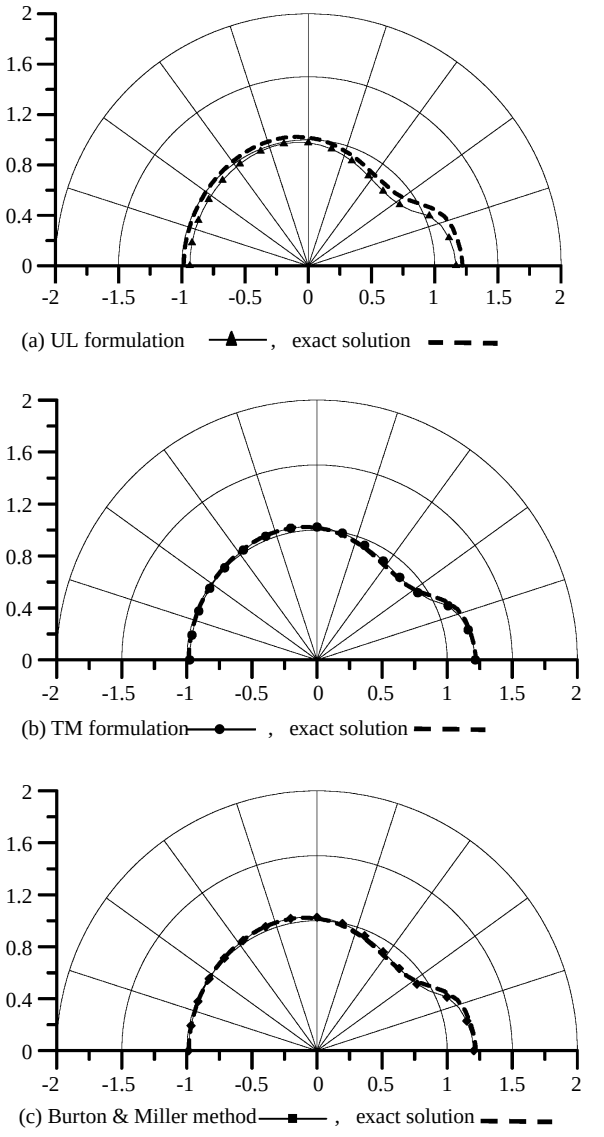

Fig. 10 Surface potential produced by the finite cylinder at interior Dirichlet eigenvalue, ka = 2.67 (2.4048/0.9), (a) UL formulation, (b) TM formulation, (c) Burton & Miller method

error compared to the analytical solution, as described in Eq. (66). Figs. 11(a)-(c) show the surface potential for k = 2.09 by using the *UL*, *TM* and mixed-layer potential method, respectively, which corresponds to the first interior Neumann eigenproblem. In Fig. 11(b) the result using the *TM* formulation shows a large error compared to the analytical solution, as described in Eq. (72).

Case 3: Plane wave scattering for a rigid infinite circular cylinder (Neumann boundary condition)

In order to check the validity of the program for the scattering problem, example 3 is considered (Harari *et al.*, 1997). The incident wave is a plane wave and the scatter is a rigid cylinder, as shown in Fig. 12. Sixty nodes are adoped for this case. The analytical solution for the scattering field is

$$u(\rho, \theta) = -\frac{J_0'(ka)}{H_0^{(1)\prime}(ka)} H_0^{(1)}(k\rho) - 2\sum_{n=1}^{\infty} i^n \frac{J_n'(ka)}{H_n^{(1)\prime}(ka)} H_n^{(1)}(k\rho)\cos(n\theta) \quad (78)$$

Figs. 13 and 14 show the contour plot for the real-part solution of MFS and analytical at $ka = 4\pi$, respectively. The results of the MFS in comparison with the analytical solution are quite good. The positions where the

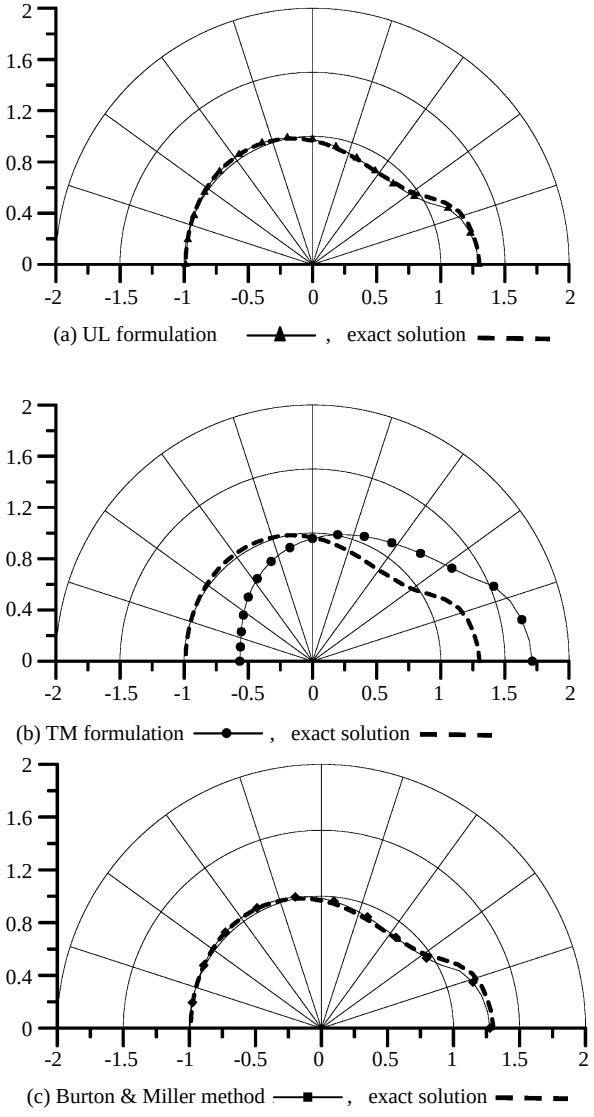

Fig. 11 Surface potential produced by the finite cylinder at interior Neumann eigenvalue, ka = 2.09 (1.84/0.9), (a) UL formulation, (b) TM formulation, (c) Burton & Miller method

irregular values occur can be found in Fig. 15 for the solution $u(a, 0; k)$ versus k. Sixty-four nodes are adoped in the MFS. The source points are located at R = 0.9 m. It is found that by using the *UL* formulation the irregular values also occur at the zeros of $J_{n,m}$. By using the *TM* formulation the irregular values also occur at the zeros of $J'_{n,m}$. The results for the MFS, analytical solution and the mixed-layer potential solution agree well, as shown in Fig. 15.

VI. CONCLUSIONS

This paper examines why fictitious frequencies occur in the MFS by considering the radiation and scattering problems of a cylinder. Based on the

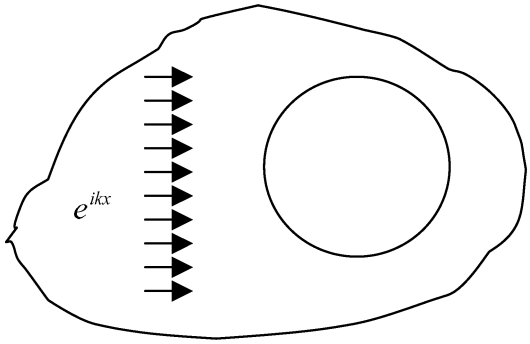

Fig. 12 The problem of a plane wave scattered by a rigid infinite circular cylinder

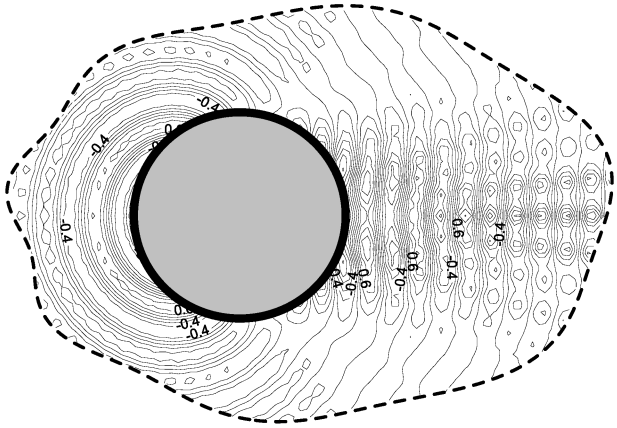

Fig. 13 The contour plot for the real-part numerical solution for a plane wave scattered by an infinite circular cylinder ($ka = 4\pi$)

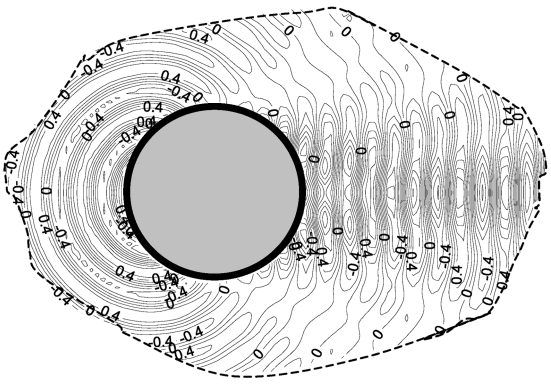

Fig. 14 The contour plot for the analytical solution for a plane wave scattered by an infinite circular cylinder ($ka = 4\pi$)

circulant properties and degenerate kernels, an analytical scheme for a discrete system of a cylinder was achieved. The occurrence of a fictitious frequency depends only on the formulation, not on the specified boundary condition. The numerical results from this study indicate that the irregular frequency also appears at the eigenvalue of the interior problem

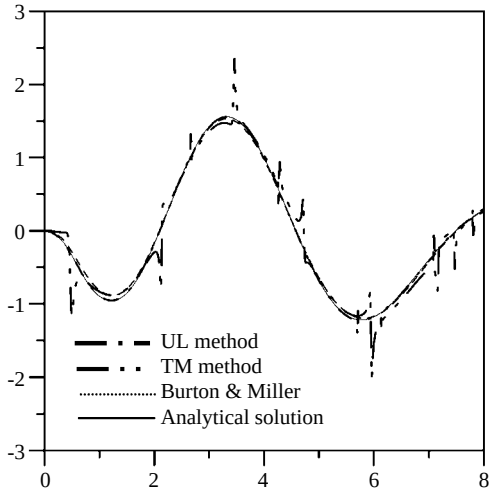

Fig. 15 The $u(a, 0; k)$ versus k using the MFS for the plane wave scattered by an infinite circular cylinder

where the boundary is connected by the source locations instead of the real boundary used in the direct BEM. In a circular cylinder case, the position of irregular frequency depends on the source location R. The mixed-layer potential method was demonstrated successfully to filter out the fictitious frequency analytically and numerically.

NOMENCLATURE

B	tbe boundary of the domain
c	sound speed
D	domain of interest
$H_n^{(1)}$	the first kind Hankel function with order n
i	$i^2 = -1$, imaginary unit
J_n	the first kind Bessel function with order n
k	wave number
$L(s, x)$	kernel function of the second dual integral eguation
$M(s, x)$	kernel function of the second dual integral eguation
n_i	the ith component of the outnormal vector at the source point s
n_x	the outnormal direction at the field point x
n_s	the outnormal direction at the source point s
$\overline{n}_i$	the ith component of the outnormal vector at field point x
r	distance between the source and field points, $r = \|x - s\|$
SVD	singular value decomposition
$T(s, x)$	kernel function of the first dual integral eguation
$t(x)$	normal flux on the field point x
$U(s, x)$	kernel function of the first dual integral eguation
$u(x)$	potential on the field point x
Y_n	the second kind Bessel function with order n
y_i	$x_i - s_i$
$\kappa, \lambda, \mu, \nu, \alpha$	eigenvalues
σ_i	singular value
φ	the mixed potential
∇^2	Laplacian operator
Γ	the vectors of undetermined coefficients
Ω	the vectors of undetermined coefficients
$\boldsymbol{\Phi}$	unitary matrix of SVD
ω	angular frequency

ACKNOWLEDGMENTS

Financial support from the National Science Council, under Grant No.NSC-92-2611-E-022-004 is gratefully acknowledged.

REFERENCES

Atluri, S. N., and Zhu T., 1998, "A New Meshless Local Petrov-Galerkin (MLPG) Approach in Computational Mechanics," *Computational Mechanics*, Vol. 22, pp. 117-127.

Belystcho, T., Lu, Y., and Gu, L., 1994, "Element Free Galerkin Methods," *International Journal for Numerical Methods in Engineering*, Vol. 37, pp. 229-256.

Burton, A. J., and Miller, G. F., 1971, "The Aplication of Integral Equation Methods to Numerical Solutions of Some Exterior Boundary Value Problems," *Proceedings of the Royal Society London Ser A*, Vol. 323, pp. 201-210.

Chen, C. S., Rashed, Y. F., and Golberg, M. A., 1998, "A Mesh-Free Method for Linear Diffusion Equations," *Numerical Heat Transfer*, Part B, Vol. 33, pp. 469-486.

Chen, J. T., 1998, "On Fictitious Frequencies Using Dual Series Representation," *Mechanics Research Communications*, Vol. 25, No. 5, pp. 529-534.

Chen, J. T., Chen, I. L., and Lee, Y. T., 2005, "Eigensolutions of Multiply-Connected Membranes Using Method of Fundamental Solution," *Engineering Analysis with Boundary Elements*, Vol. 29, pp. 166-174.

Chen, J. T., Chen K. H., Chen, I. L., and Liu, L. W., 2003, "A New Concept of Modal Participation Factor for Numerical Instability in the Dual BEM for Exterior Acoustics," *Mechanics Research Communications*, Vol. 30, pp. 161-174.

Chen, J. T., and Kuo, S. R., 2000, "On Fictitious Frequencies Using Circulants for Radiation Problems of a Cylinder," *Mechanics Research Communications*, Vol. 27, No. 3, pp. 49-58.

Chen, J. T., Kuo, S. R., Chen, K. H., and Cheng, Y. C., 2000, Comments on Vibration Analysis of Arbitrary Shaped Membranes Using Nondimensional Dynamic Influence Function," *Journal of Sound and Vibration*, Vol. 235, No. 1, pp. 156-171.

Cisilino, A. P., and Sensale, B., 2002, "Application of a Simulated Annealing Algorithm in the Optimal Placement of the Source Points in the Method of the Fundamental Solutions," *Computational Mechanics*, Vol.28, pp.129-136.

Dokumaci, E., 1990, "A Study of the Failure of Numerical Solutions in Boundary Element Analysis of Acoustic Radiation Problems," *Journal of Sound and Vibration*, Vol. 139, No. 1, pp. 83-97.

Fairweather, G., and Karageorghis, A., 1998, "The Method of Fundamental Solutions for Elliptic Boundary Value Problems," *Advances in Computational Mathematics*, Vol. 9, pp. 69-95.

Fairweather, G., Karageorghis, A., and Martin, P. A., 2003, "The Method of Fundamental Solutions for Scattering and Radiation Problems," *Engineering Analysis with Boundary Elements*, Vol. 27, pp. 759-769.

Gingold, R. A., and Maraghan, J. J., 1977, "Smoothed Particle Hydrodynamics: Theory and Applications to Non-Spherical Stars," *Monthly Notices of the Royal Astronomical Society*, Vol. 181, pp. 375-389.

Golberg, M. A., Chen, C. S., and Ganesh, M., 2000, "Particular Solutions of 3D Helmholtz-Type Equations Using Compactly Supported Radial Basis Functions," *Engineering Analysis with Boundary Element*, Vol. 24, pp. 539-547.

Harari, I., Barbone, P. E., Slavutin, M., and Shalom, R., 1998, "Boundary Infinite Elements for the Helmholtz Equation in Exterior Domains," *International Journal for Numerical Methods in Engineering*, Vol. 41, pp. 1105-1131.

Harari, I., Barbone, P. E., and Montgomery, J. M., 1997, "Finite Element Formulations for Exterior Problems: Application to Hybrid Methods, Non-Reflecting Boundary Conditions, and Infinite Elements," *International Journal for Numerical Methods in Engineering*, Vol. 40, pp. 2791-2805.

Hwang, J. Y., and Chang, S. C., 1991, "A Retracted Boundary Integral Equation for Exterior Acoustic Problem with Unique Solution for All Wave Numbers," *Journal of the Acoustical Society of America*, Vol. 90, pp. 1167-1180.

Kondapalli, P. S., Shippy, D. J., and Fairweather, G., 1992, "Analysis of Acoustic Scattering in Fluids and Solids by the Method of Fundamental Solutions," *The Journal of Acoustical Society of America*, Vol. 91, No. 4, pp. 1844-1854.

Kuo, S. R., Chen, J. T., and Huang, C. X., 2000, "Analytical Study and Numerical Experiments for True and Spurious Eigensolutions of a Circular Cavity Using the Real-Part Dual BEM," *International Journal for Numerical Methods in Engineering*, Vol. 48, No. 9, pp. 1401-1422.

Lee, C. -H., Newman, J. N., and Zhu, X., 1996, "An Extended Boundary Integral Equation Method for the Removal of Irregular Frequency Effects," *International Journal for Numerical Methods in Fluids*, Vol. 23, pp. 637-660.

Lee, C. -H., and Sclavounos, P. D., 1989, "Removing the Irregular Frequencies from Integral Equation in Wave-Body Interactions," *Journal of Fluid Mechanics*, Vol. 207, pp. 393-418.

Liu, W. K., Jun, S., and Zhang, Y. F., 1995, "Reproducing Kernel Particle Methods," *International Journal for Numerical Methods in Engineering*, Vol. 20, pp. 1081-1106.

Malenica, S., and Chen, X. B., 1998, "On the Irregular Frequencies Appearing in Wave Diffraction-Radiation Solutions," *International Journal of Offshore and Polar Engineering*, Vol. 8, No. 2, pp. 110-114.

Mukherjee, Y. X., and Mukherjee, S., 1997, "The Boundary Node Method for Potential Problems," *International Journal for Numerical Methods in Engineering*, Vol. 40, pp. 797-815.

Ohmatsu S., 1983, " A New Simple Method to Eliminate the Irregular Frequencies in the Theory of Water Wave Radiation Problems," *Papers of Ship Research Institute*, Vol. 70.

Poullikkas, A., Karageorghis, A., and Georgiou, G., 2002, "The Method of Fundamental Solutions for Three-Dimensional Elastostatics Problems," *Computers and Structures*, Vol. 80, pp. 365-370.

Ramachandran, P. A., 2002, "Method of Fundamental Solutions: Singular Value Decomposition Analysis," *Communications in Numerical Methods in Engineering*, Vol. 18, pp. 789-801.

Sladek, V., Sladek, J., Atluri, S. N., and Van Keer R., 2000, "Numerical Integration of Singularities in Meshless Implementation of Local Boundary Integral Equations," *Computational Mechanics*, Vol. 25, pp. 394-403.

Ursell, F., 1981, "Irregular Frequencies and the Motions of the Floating Bodies," *Journal of Fluid Mechanics*, Vol. 143, pp. 143-156.

Zhang, X., Song, K. Z., Lu, M. W., and Liu, X., 2000, "Meshless Methods Based on Collocation with Radial Basis Functions," *Computational Mechanics* Vol. 26, pp. 333-343.

Manuscript Received: Jan. 05, 2005
Revision Received: May 16, 2005
and Accepted: Jun. 30, 2005